

## Supporting Information:

### Determining the Role of Oxygen Vacancies in the Photoelectrocatalytic Performance of WO<sub>3</sub> for Water Oxidation

Sacha Corby<sup>1,2</sup>, Laia Francàs<sup>1</sup>, Andreas Kafizas<sup>1,2</sup> and James R. Durrant<sup>1\*</sup>

<sup>1</sup>Department of Chemistry and Centre for Plastic Electronics, Imperial College London, White City Campus, London, W12 0BZ, UK

<sup>2</sup>Grantham Institute for Climate Change, Imperial College London, South Kensington, London, SW7 2AZ, UK

\*corresponding: [j.durrant@imperial.ac.uk](mailto:j.durrant@imperial.ac.uk)

#### Contents

A – Preparation of WO <sub>3</sub> photoanodes	2
B – [Vo] modifications	2
C – Photoelectrochemical measurements	2
D – Optical measurements	3
E – Imaging	4
F – XRD data	5
G – XPS data on oxygen vacancies	6
H – Photocurrent data	8
I – Additional kinetic data	11
J – References	13

## A – Preparation of WO<sub>3</sub> films

WO<sub>3</sub> needles (approx. 4 μm long x 100 nm diameter) were grown on top of a dense WO<sub>3</sub> seed layer (400 nm thick) on FTO coated glass using aerosol-assisted chemical vapour deposition (AA-CVD), in a procedure detailed by Kafizas *et al.*<sup>1</sup> The needles were formed by heating the apparatus to 375 °C, with a carrier gas (N<sub>2</sub>) flow rate of 300 sccm, whereas the seed layer was formed at 325 °C with a flow rate of 180 sccm. The synthesised films were monoclinic, with growth almost exclusively in the (002) direction and deep blue in colour due to a high concentration of oxygen vacancies. The films were then annealed at 500 °C in air for two hours, unless otherwise specified, resulting in characteristic pale-yellow WO<sub>3</sub>.

## B - [V<sub>O</sub>] modification

Four different sample types were used in this work and referred to as ‘very high’, ‘high’, ‘medium’ and ‘low’ in accordance with the oxygen vacancy concentration in each. Samples with ‘very high’ vacancy concentrations were the product of the deposition method itself, and thus no further treatment was required (*i.e.* the films were not annealed and used as-prepared). The high defectiveness of these films can be readily observed by XPS, which reveals a high W<sup>5+</sup>:W<sup>6+</sup> ratio of 0.35, *i.e.* more than a third of the tungsten atoms probed were in a reduced state due to neighbouring oxygen vacancies (Figure S1a). Samples reported herein as ‘high’ in [V<sub>O</sub>] were attained by annealing the as-deposited material for 2 hours at 500 °C in air before exposing to acid (0.1 M H<sub>2</sub>SO<sub>4</sub>). The films were allowed to dry at room temperature and were then annealed again for 1 hour under otherwise comparable conditions. This procedure consistently produced tungsten oxide films with higher oxygen-vacancy concentrations (2.3% [V<sub>O</sub>]) than regular annealing, possibly due to co-adsorbed hydrogen from the acid (though hydrogen could not be detected).<sup>2,3</sup> Samples with lower concentrations of defect states were obtained by altering the annealing time. WO<sub>3</sub> films with ‘medium’ [V<sub>O</sub>] (Figure S2c) were annealed for 2 hours, as studied in previous work,<sup>4</sup> whereas films with almost perfect stoichiometric ratios of oxygen to tungsten (0.5% [V<sub>O</sub>]), herein named ‘low’, were the product of a 12 hour anneal to allow oxygen to permeate deep into the lattice structure.

An additional hydrogen annealing treatment was performed in order to add vacancies back into the annealed films as a proof of the reversibility of the performance trends discussed in the manuscript. This annealing involved heating the samples at 300°C in an atmosphere of 10% H<sub>2</sub> in N<sub>2</sub> for 1 hour (Figure S7).

## C – Photoelectrochemical measurements

All photoelectrochemical analyses were conducted using a three-electrode set up in 0.1 M H<sub>2</sub>SO<sub>4</sub> (pH 1) electrolyte prepared from concentrated H<sub>2</sub>SO<sub>4</sub> (Reagent grade, Sigma Aldrich) and Milli-Q water (Millipore Corp., 18.2 MΩ.cm, 25°C). Pt gauze was used as the counter electrode and a Ag/AgCl/saturated KCl (Metrohm) was used as the reference electrode (E° = +0.197 V vs NHE). All potentials are referenced against the reversible hydrogen electrode

(RHE) by use of the Nernst equation. The home-made PTFE cell has a quartz window of 0.503 cm<sup>2</sup> and each WO<sub>3</sub> working electrode in this study was irradiated from the front (EE; electrode-electrolyte) unless otherwise stated. The cell was connected to an Autolab (PGSTAT101) potentiostat and the scan rate was 10 mV/s for all linear sweep voltammograms. The irradiation source was a 75 W Xenon arc lamp, modulated with neutral density filters to provide approximately 100 mW/cm<sup>2</sup> (1 Sun) intensity.

## D – Optical measurements

Ultrafast Transient Absorption Spectroscopy (TAS) was conducted on the femtosecond to nanosecond timescale using a regeneratively amplified Ti:sapphire laser system (Solstice, Spectra-Physics) and Helios spectrometers (Ultrafast Systems), which generates 800 nm laser pulses (pulse width: 92 fs, repetition rate: 1 kHz). To generate the pump, a fraction of the 800 nm beam was directed through a sequence of optical parametric amplifier (TOPAS Prime, Spectra-Physics) and a frequency mixer (NIR/UV-Vis, Light Conversion) to tune the excitation wavelength to 355 nm. The intensity of the pump was modulated using neutral density filters, and measured using an energy meter (VEGA, P/N 7Z01560, OPHIR Photonics), fitted with a 0.5 mm diameter aperture. The pump beam at the sample was  $\geq 0.5$  mm. A visible white light continuum (WLC) was used as the probe, generated from a fraction of the 800 nm pulse, focused onto a Ti:sapphire crystal. The probe beam was delayed with respect to the pump beam using a motorised delay stage to alter the path length of the probe beam before generation of the WLC. To reduce the noise, the WLC was split into two beams, one of which is passed through the sample, and the other used as a reference. Both beams were subsequently focused onto separate fibre-optic coupled, multichannel spectrometers (CMOS sensors). Alternate pump pulses were blocked using a synchronised chopper (500 Hz). As such, absorption spectra of the excited and unexcited sample were obtained to determine the time-resolved absorption difference spectrum. Time zero was then adjusted to match the rise of the signal at each wavelength. The presented decay kinetics were averaged over a spectral range of *ca.* 10 nm.

The slower kinetic data presented herein were obtained by transient diffuse reflectance spectroscopy (TDRS)<sup>5</sup> on a home-built system, as the WO<sub>3</sub> needles were scattering. Samples were examined under bias using the PEC setup described above and a cell with a larger quartz window. The excitation source was an Nd:YAG laser (OPOTEK Inc, Opolette 355 II) firing at the third harmonic, 355 nm, with a 6 ns pulse width. The laser excitation power density was kept constant at 280-340  $\mu\text{J}/\text{cm}^2$  and the frequency was 0.4 Hz. A liquid light guide with a diameter of 0.5 cm was used to transmit the laser pulse to the sample. The continuous probe beam was generated from a 100 W Bentham IL1 quartz halogen lamp and passed through selected long pass filters (Thorlabs) to remove short wavelengths before irradiating the sample. An IR filter (H<sub>2</sub>O, 5 cm path length) was used to prevent heating of the sample. A series of mirrors were used to angle the diffuse reflected light from the sample through a monochromator (Oriel

Cornerstone 130) to select the probe wavelength and on to a silicon photodiode detector (Hamamatsu S3071). Data from 1  $\mu$ s to 3 ms was passed through an amplifier box (Costronics) and recorded using an oscilloscope (Tektronics DPO3012). Data from 3 ms to 1 s was recorded using a National Instruments DAQ card (NI USB-6211). The change in the percentage absorbance is calculated from the detected signal using LabView software. The transient photocurrent signal was measured simultaneously via the oscilloscope during the measurement to provide information on the electron extraction. Each optical and photocurrent decay presented in this work is the average of 50-100 laser pulses.

## E – Imaging

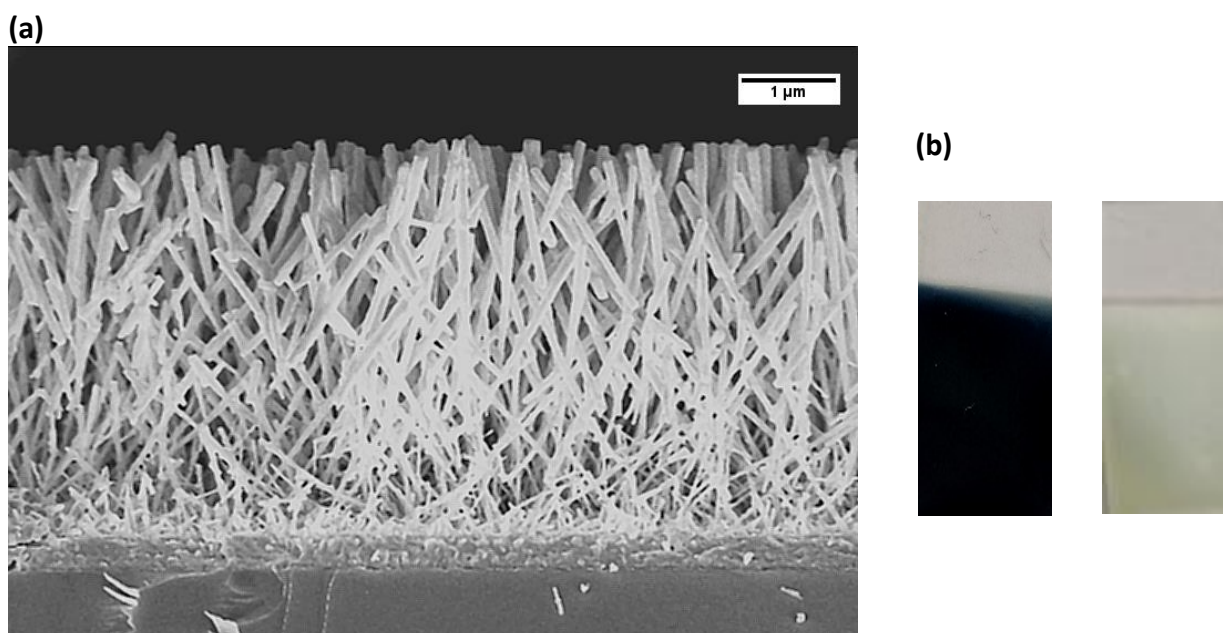


Figure S1: (a) SEM image of  $\text{WO}_3$  needles (2-hours annealed) and (b) photographs of samples on FTO, before (blue) and after (yellow) annealing (1.2 cm x 2.2 cm).

## F – XRD data

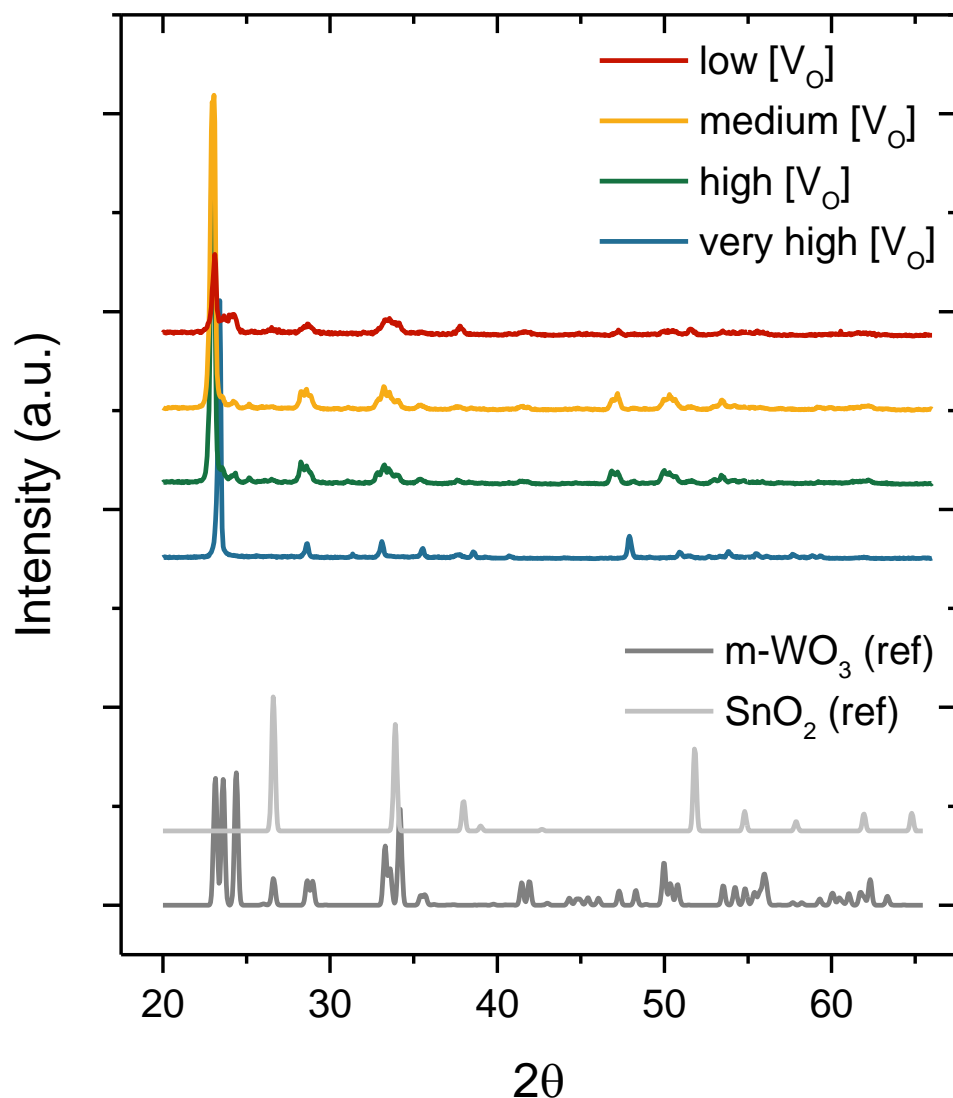


Figure S2: X-ray diffraction data for each of the films studied. Monoclinic WO<sub>3</sub> and SnO<sub>2</sub> (FTO) references are provided. No additional phases are observed.

We note that subtle changes in crystallinity may be detected between the different samples, with the as-prepared 'very high' [V<sub>O</sub>] sample most crystalline. In order to rule out any significant effect from changes in crystallinity, we annealed the 'medium' and 'low' [V<sub>O</sub>] samples in 10% H<sub>2</sub> to add vacancies back into the samples. This gave the expected trends in performance (Figure S7), thereby confirming that oxygen vacancy concentration is the predominant factor controlling performance.

## G – XPS data on oxygen vacancies

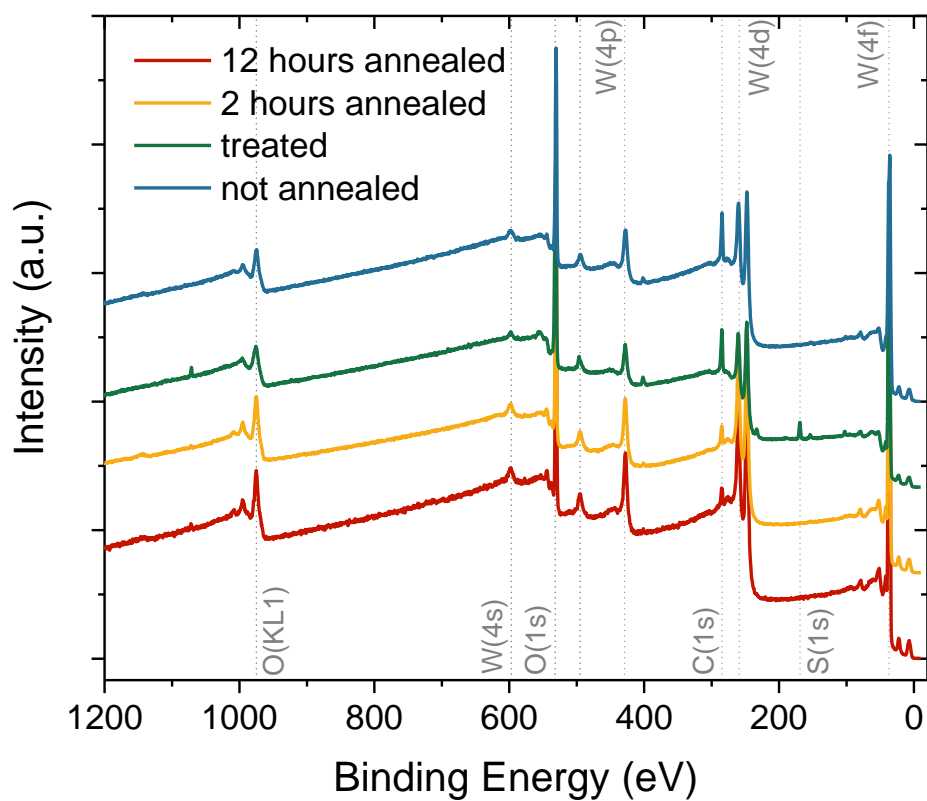


Figure S3: XPS survey scan of each of the WO<sub>3</sub> samples in the study: 12 hours annealed (low [V<sub>O</sub>], blue), 2 hours annealed (medium [V<sub>O</sub>], yellow), treated (high [V<sub>O</sub>], green) and not annealed (very high [V<sub>O</sub>], red).

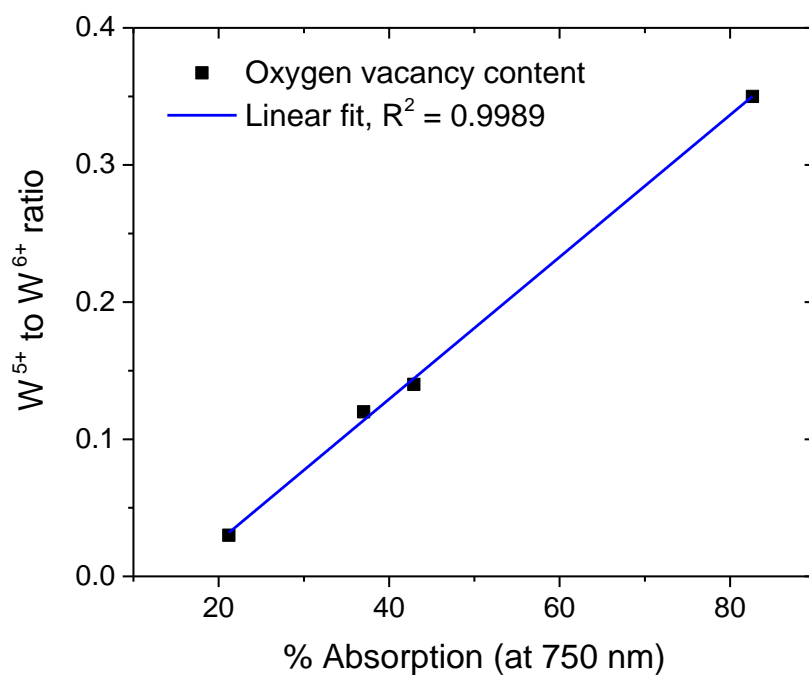


Figure S4: Linear relationship between the respective W<sup>5+</sup> content from XPS data (Figure 2) and the coloration due to the W<sup>5+</sup> absorption band (Figure 1) from the series of films analysed herein.

## H – Photocurrent data

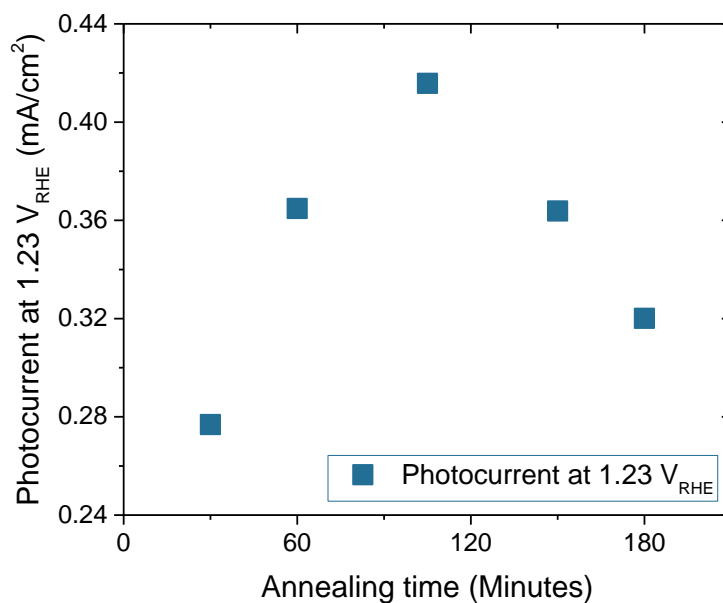


Figure S5: Photocurrent under 1 sun illumination (front side) against sample annealing time in air at 500 °C.

Unfortunately, variations in performance with annealing differed too greatly between batches for these samples to be used throughout all the kinetic analyses (which often require multiple samples owing to the stress of the experiments). Trends in performance with oxygen vacancy concentration varied to a much lesser extent in the more 'extreme' treatments used herein.

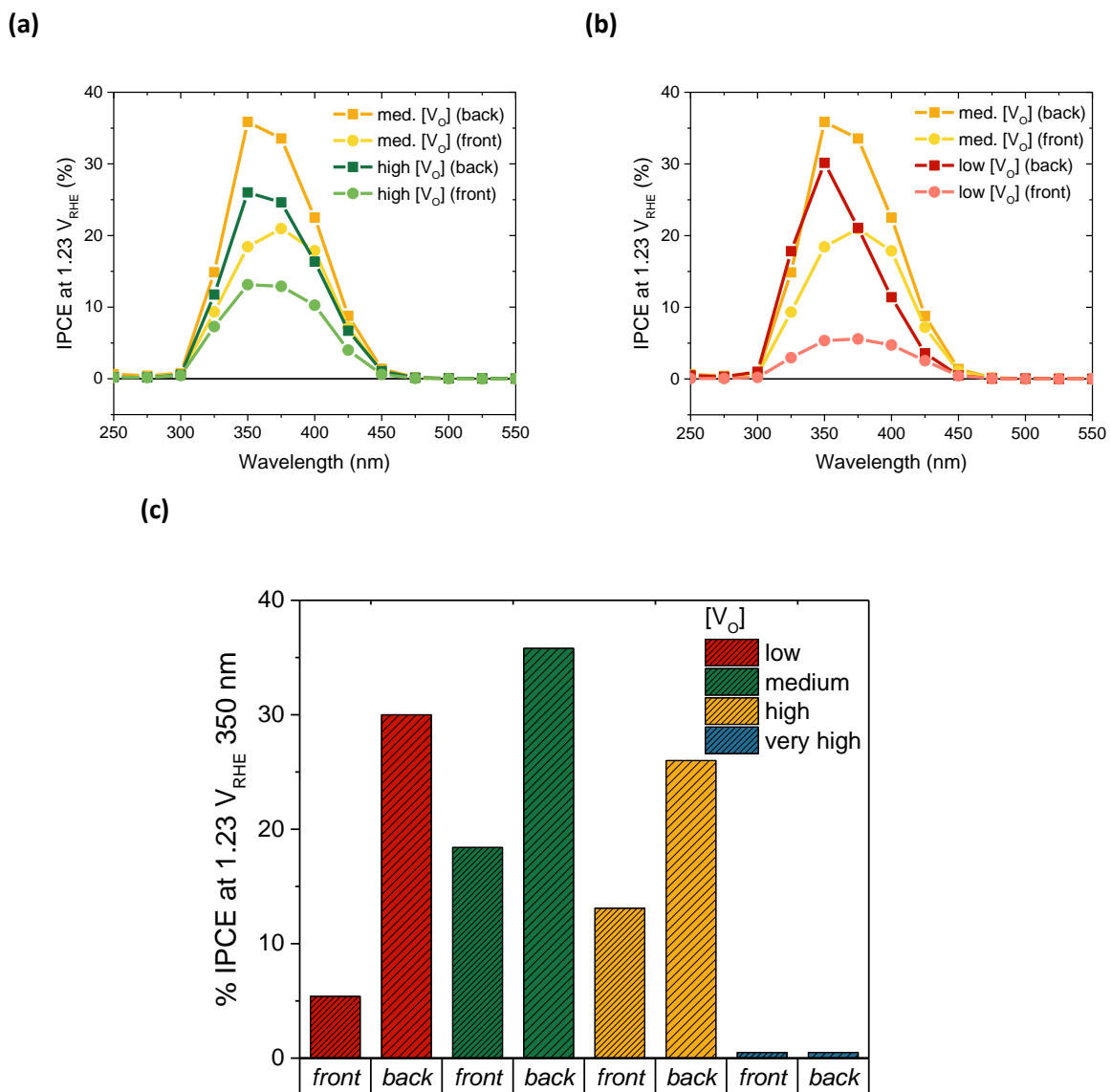
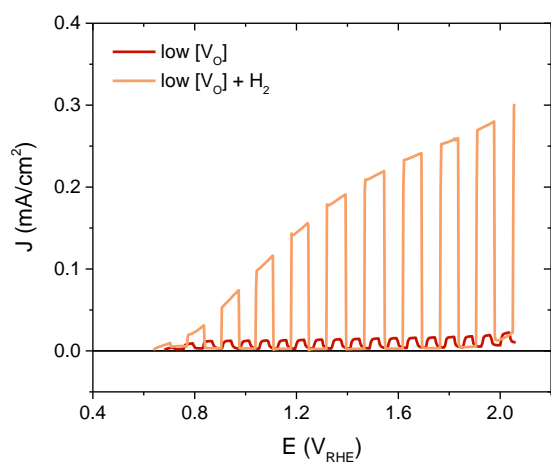


Figure S6: Incident photon-to-current efficiency (IPCE) from the front (lighter shades) and the back (darker shades) for samples with (a) 'medium' [V<sub>O</sub>] (yellow) and 'high' [V<sub>O</sub>] (green), and (b) 'medium' [V<sub>O</sub>] (yellow) and 'low' [V<sub>O</sub>] (red). (c) Bar chart of the same data for alternative comparison.

(a)



(b)

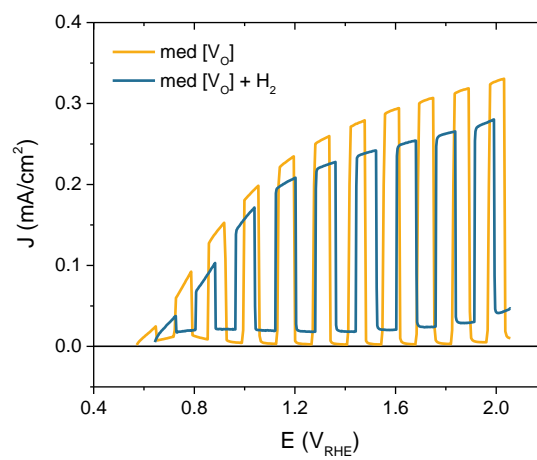


Figure S7: Chopped LSV scans before and after annealing the (a) 'low' and (b) 'medium'  $[V_o]$  samples in a reducing atmosphere to create additional oxygen vacancies.

## I – Additional Kinetic Data

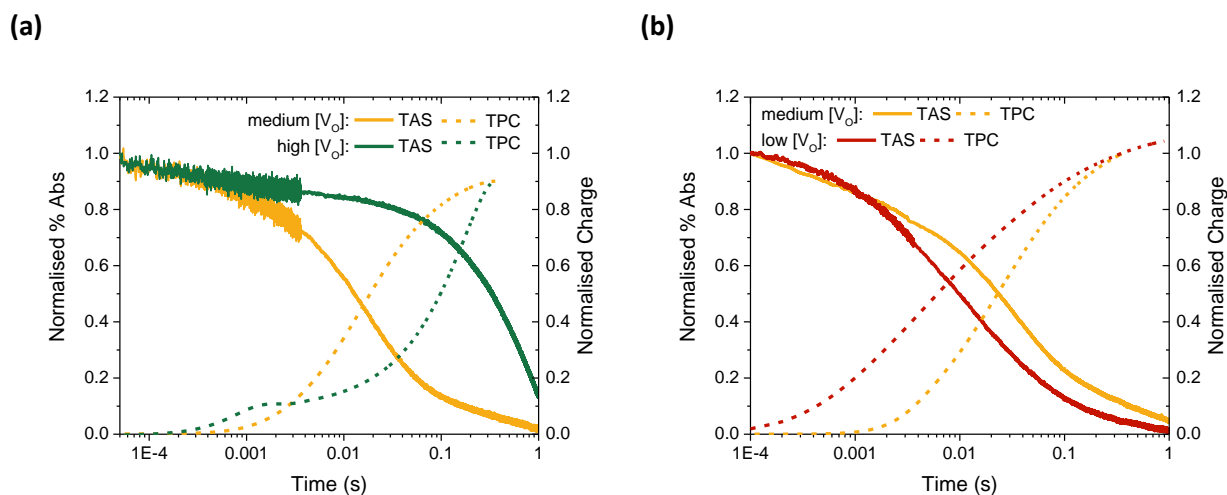


Figure S8: Normalised kinetic traces at 800 nm from the data presented in Figure 4 in the main article, comparing (a) 'high' (green) and 'medium' (yellow) doping, and (b) 'medium' (yellow) and 'low' (red) doping. Separated for ease of viewing.

Table S1: External quantum yields calculated from transient photocurrent data in Figure 4

WO <sub>3</sub> Sample	External Quantum Yield
'high'	1.7 %
'medium'	9.4 %
'low'	1.0 %

External quantum yields were calculated as follows:

Pulse intensity = 0.25 mJ/cm<sup>2</sup>

Pulse wavelength = 355 nm

Pulse energy  $\rightarrow E = hc/\lambda = 5.6 \times 10^{-19}$  J

# photons  $\rightarrow$  intensity/energy =  $4.47 \times 10^{14}$  photons/cm<sup>2</sup>

# electrons = # photons =  $4.47 \times 10^{14}$  photogenerated electrons/cm<sup>2</sup>

Theoretical charge  $\rightarrow$  # electrons x charge of 1 electron =  $7.1 \times 10^{-5}$  C = 71  $\mu$ C/cm<sup>2</sup>

Extracted charge ('medium' [V<sub>o</sub>]) = 6.7  $\mu$ C/cm<sup>2</sup> (see Figure 4)

EQE = extracted/theoretical x 100 = 9.4 %

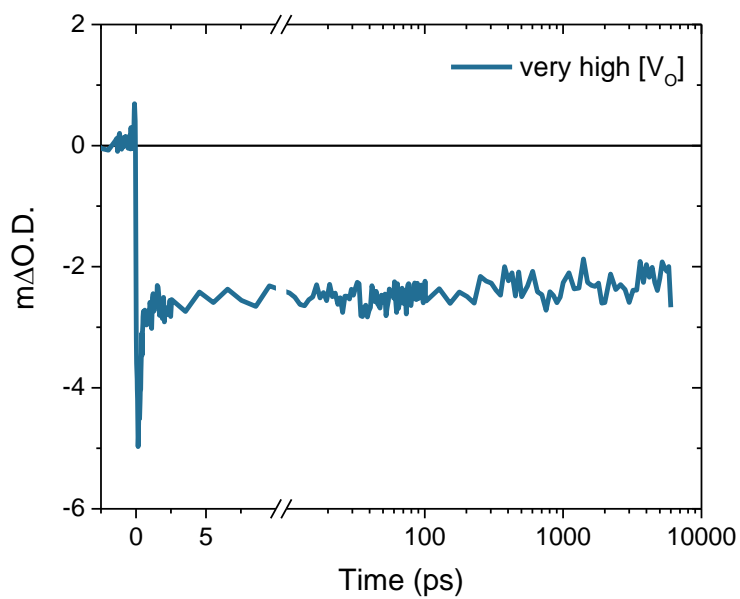


Figure S9: Ultrafast kinetic data at 740 nm for the highest doped sample, revealing that no positive signal from electron trapping is observed as most of the oxygen vacancy states now lie below the Fermi level and thus trap holes, which deplete the  $W^{5+}$  absorption, rather than electrons.

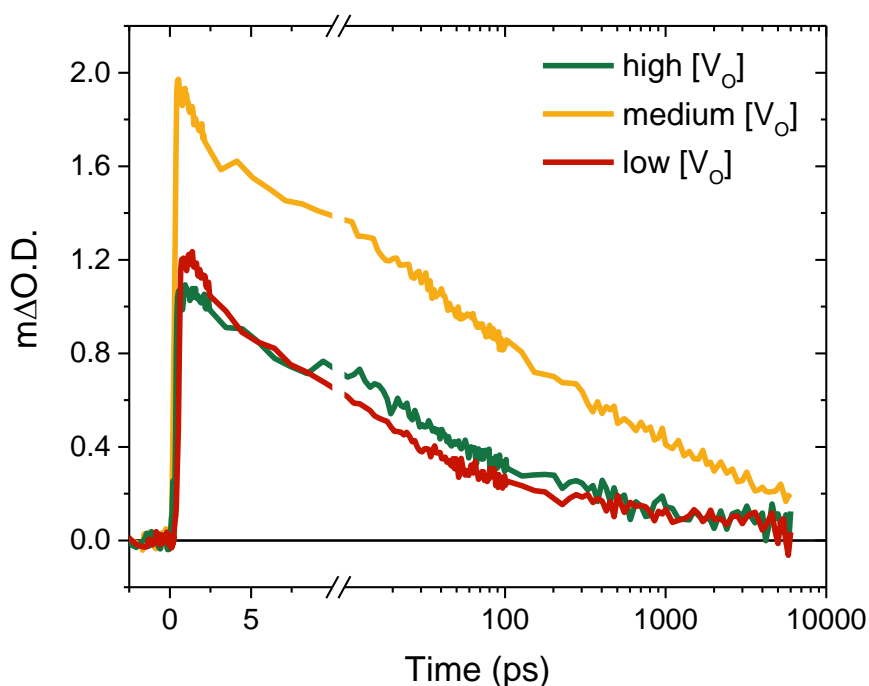


Figure S10: Ultrafast kinetics of electrons at 800 nm, as shown normalised in Figure 5 in the main article. Measuring absolute amplitudes in highly reflective samples can be challenging, but this data suggests that the ‘high’  $[V_o]$  and ‘low’  $[V_o]$  samples suffer immediate recombination losses at timescales faster than we can resolve. We assign this to poorer charge separation, leading to increased trapped-mediated loss in the highly doped sample, and increased ‘geminate-style’ recombination in the poorly doped sample, as discussed in the main article.

## J - References

- (1) Kafizas, A.; Francàs, L.; Sotelo-Vazquez, C.; Ling, M.; Li, Y.; Glover, E.; McCafferty, L.; Blackman, C.; Darr, J.; Parkin, I. *The Journal of Physical Chemistry C* **2017**, *11*, 5983.
- (2) Liu, G.; Han, J.; Zhou, X.; Huang, L.; Zhang, F.; Wang, X.; Ding, C.; Zheng, X.; Han, H.; Li, C. *Journal of Catalysis* **2013**, *307*, 148.
- (3) Johansson, M. B.; Kristiansen, P. T.; Duda, L.; Niklasson, G. A.; Österlund, L. *Journal of Physics: Condensed Matter* **2016**, *28*, 475802.
- (4) Corby, S.; Francàs, L.; Selim, S.; Sachs, M.; Blackman, C.; Kafizas, A.; Durrant, J. R. *Journal of the American Chemical Society* **2018**, *140*, 16168.
- (5) Wilkinson, F. *Journal of the Chemical Society, Faraday Transactions 2: Molecular and Chemical Physics* **1986**, *82*, 2073.